Evaluation of Optical Proxies for Suspended Particulate Mass in Stratified Waters

Jing Tao and Paul S. Hill

Dalhousie University, Halifax, Nova Scotia, Canada

Emmanuel S. Boss

School of Marine Sciences, University of Maine, Orono, Maine

Timothy G. Milligan

Bedford Institute of Oceanography, Dartmouth, Nova Scotia, Canada

ABSTRACT

Optical instruments that measure the particulate beam attenuation (c_p) and backscattering coefficients (b_{bp}) have been used widely to estimate suspended particulate mass (SPM) in various environments. In pycnoclines, density differences can cause significant forward light scattering (schlieren). This fluid-induced scattering increases the c_p measured by instruments with small acceptance angles that are open to the environment (not pumped). When the 1-m bin-averaged buoyancy frequency (N) exceeds $0.05\,\mathrm{s}^{-1}$ in the Columbia River estuary, inaccurate estimates of c_p are observed by such instruments. The schlieren phenomena do not affect the c_p and b_{bp} measured with a pumped transmissometer or a backscattering meter. It follows that to obtain a reliable proxy of SPM in a highly stratified environment, the use of either a backscattering sensor or a pumped transmissometer is required.

1. Introduction

Optical instruments provide useful proxies for particle properties in the ocean (e.g., Boss et al. 2004, 2015; Braithwaite et al. 2010; Hill et al. 2011, 2013b). Optical sensors are used to assess suspended particulate mass (SPM) concentration because it is impractical to take water samples at the spatial and temporal scales at which systems are forced (Boss et al. 2009c). The advantage of optical measurements is that they provide an automated, continuous time series of proxies for SPM at inaccessible locations or in environments with rapidly changing SPM (Schoellhamer and Wright 2003). SPM is typically correlated linearly with the particulate beam attenuation coefficient, the backscattering coefficient, or the side-scattering coefficient across a range of

environments (e.g., Boss et al. 2009b; Hill et al. 2011; Neukermans et al. 2012).

The correlation between particulate beam attenuation (c_p) and SPM in stratified waters can be degraded significantly by light scattering induced by differences in the refractive indexes of different water masses. The light scattering creates a phenomenon called *schlieren*, which are filaments of higher or lower density water that cause refraction of light (Styles 2006; Mikkelsen et al. 2008; Karageorgis et al. 2015).

In previous studies the failure to consider the effects of schlieren on light scattering may have produced erroneous inferences of particle-rich layers in pycnoclines across a range of environments. For example, Kistner and Pettigrew (2001) observed dramatic increases in attenuation at 2 psu in the Kennebec River estuary in Maine that they attributed to the accumulation of SPM in an estuarine turbidity maximum (ETM). In general in the estuary, attenuation and salinity were inversely linearly correlated, indicating that simple mixing of particle-laden riverine waters with particle-depleted coastal waters determined the optical attenuation. The significant deviation from this linear

Corresponding author: Jing Tao, jing.tao@dal.ca

correlation at 2 psu may have been due to a mixing-induced effect on optical attenuation rather than by accumulation of SPM in the ETM. Jones et al. (2002) used a towed transmissometer to examine the vertical distribution of sediment in the water column of the Palos Verdes continental shelf in California. Interestingly, the depth of the largest variance of c_p was associated with the depth of the maximum density gradient, suggesting that schlieren effects may have been misinterpreted as particle-rich layers. In the Cariaco Basin on the Venezuelan continental shelf, peaks in vertical profiles of beam attenuation were interpreted as internal nepheloid layers (INLs) that played a role in the redistribution of organic matter in the basin (Lorenzoni et al. 2009). The attenuation peaks, however, generally occurred in pycnoclines, so they may have been due to the mixing of waters of different density rather than elevated particle concentrations. In these studies and others, the lack of other observations precludes the resolution of whether particle-rich layers were real or an artifact of light scattering by schlieren.

INLs and ETMs may have been falsely identified because of schlieren, leading to the misunderstanding of sediment dynamics in stratified environments. INLs and ETMs are important for particle transport from the continents to the ocean basins. INLs are associated with strong density gradients and carry significant quantities of suspended particles over long distances, from coastal environments to the deep sea (Puig et al. 2004; Lorenzoni et al. 2009). The trapping of particles in ETMs increases the residence time of particles in estuaries, which can accelerate metabolic processes in estuarine ecosystems (Kappenberg et al. 1995; Burchard and Baumert 1998; North et al. 2004).

The Laser In Situ Scattering and Transmissometry (LISST-100x) instrument developed by Sequoia Scientific Inc. has been used widely to estimate particle size distribution, volume concentration, and mass in coastal waters (e.g., Fugate and Friedrichs 2002; Traykovski et al. 2004; Hill et al. 2011; Neukermans et al. 2012), but it is affected strongly by schlieren. In a laboratory study, Styles (2006) evaluated the performance of LISST-100x in a stratified environment. He showed that density stratification could produce results similar to scattering because of particles, resulting in overestimated concentrations for larger particles in the pycnocline. Both Mikkelsen et al. (2008) and Karageorgis et al. (2015) evaluated the LISST in coastal waters in the context of buoyancy frequency profiles, where the buoyancy frequency essentially is a measure of the vertical density gradient in the water column. Mikkelsen et al. (2008)

found that buoyancy frequencies above $0.025\,\mathrm{s}^{-1}$ were associated with increases in beam attenuation because of schlieren. Karageorgis et al. (2015) suggested that a buoyancy frequency of $0.01\,\mathrm{s}^{-1}$ is the appropriate threshold for schlieren occurrence for LISST. According to Karageorgis et al. (2015), above these thresholds the LISST artifacts cannot be avoided, but they can be removed manually by estimation of the buoyancy frequency. Unfortunately, the threshold buoyancy frequencies are relatively low, which restricts the use of LISST measurements for estimation of SPM in many environments.

Mikkelsen et al. (2008) and Karageorgis et al. (2015) showed that other sensors are less affected by schlieren than the LISST. Specifically, instruments with larger acceptance angles do not detect some light scattered in the very near-forward direction as scattered but rather as transmitted. Schlieren primarily affect scattering in the very near-forward direction, so small changes to the angular scattering pattern are not detected as strongly by instruments with larger acceptance angles. In a study in Hudson Bay, Xi et al. (2014) assumed that a larger acceptance angle transmissometer was not prone to schlieren effects, and based on this assumption they eliminated LISST observations of beam attenuation that were significantly larger than the observations from the other instrument. They determined that spurious LISST data were concentrated in pycnoclines near the coast. Despite the apparent effectiveness of Xi et al.'s (2014) approach, both Mikkelsen et al. (2008) and Karageorgis et al. (2015) showed that larger-acceptance-angle transmissometers such as those used in the studies of INL and ETM discussed above can be affected by schlieren, so their usefulness as proxies for SPM in stratified waters is also restricted.

Two possible alternative optical proxies for SPM in stratified waters are attenuation coefficients in pumped sensors or optical backscattering coefficients. In pumped systems density gradients likely would be mixed in the intake, which would destroy the conditions for schlieren to form. Because schlieren affect near-forward scattering, backscattering coefficients should not be affected by schlieren and should remain good proxies for SPM in stratified waters. The goal of this research is to compare three different optical proxies for SPM and to determine their utility as SPM proxies in a highly stratified estuary: the beam attenuation coefficient at 670 nm from a LISST-100x type B (acceptance angle of 0.027°), the beam attenuation coefficient at 650 nm from a WET Laboratories ac-9 (acceptance angle of 0.93°, pumped system), and the backscattering coefficient at 650 nm from a WET

Laboratories Environmental Characterization Optics (ECO) bb2fl (measures scattering at an angle of 124°).

2. Materials and methods

The highly stratified Columbia River estuary (CRE), separating Oregon and Washington, is strongly affected by large tidal currents, strong winds, and seasonally varying river discharges, all of which influence the sediment dynamics (Elias et al. 2012). Measurements were made with a profiling instrument package in the CRE. The instrument package carried a Sequoia Scientific LISST-100x type B (LISST), a machine vision floc camera (MVFC), a WET Laboratories ac-9 absorption and attenuation sensor with a 10-cm pathlength, a WET Laboratories ECO bb2fl, a WET Laboratories WETStar colored dissolved organic matter (CDOM) fluorometer, an RBR CTD, a Sea-Bird 37 CTD, and two pressure-actuated Niskin bottles. Data were collected on 44 descending profiles along the estuary, extending approximately 40 km upstream from the river mouth bar out onto the adjacent continental shelf. Particle and optical properties were measured in vertical profiles with a profiling speed of $0.5 \, \mathrm{m \, s^{-1}}$. Measurements were made from R/V *Point Sur* during relatively high discharge conditions during 1–5 June 2013. Daily averaged flow was $8930 \, \mathrm{m^3 \, s^{-1}}$ at Beaver Army Terminal during the measuring period, and annual mean flow is $7300 \, \mathrm{m^3 \, s^{-1}}$ (Bottom et al. 2005).

Marine particles often are packaged in aggregates for which mass is proportional not to volume, as it is in solid spheres, but instead is proportional to area (Hill et al. 1994; Boss et al. 2009a; Hill et al. 2011). This particle packing geometry explains why optical properties can be used as proxies for SPM. In short, because particulate beam attenuation and scattering are proportional to the projected area concentration of the particles in suspension (e.g., Beardsley et al. 1970; Pak and Zaneveld 1977), they also are proportional to SPM (Boss et al. 2009a; Hill et al. 2011).

To examine the effect of schlieren on the accuracy of optical proxies for SPM, we first compared the optical proxies to total particle area concentration (TAC, $\mathrm{m^{-1}}$) in suspension. Comparing optical proxies to TAC maximizes the amount of data, and it avoids any effects associated with the violation of the assumption that particle mass is proportional to particle area. The TAC is calculated by integrating the particle size distribution (PSD) of the area concentration over a full range of particle diameters. The PSD of the area concentration was estimated with the LISST and the MVFC in this study. The LISST and MVFC PSDs were merged to produce size spectra that covered the in situ particle size

ranging from 2.85 to $540 \, \mu\mathrm{m}$ (Mikkelsen et al. 2005). The LISST uses small angle forward laser light scattering to retrieve the in situ volume distribution of suspended particles. The LISST sampled continuously while in the water, and 2-s average PSDs comprising 50 samples were computed using the manufacturer-provided software. LISST data were processed in MATLAB (The MathWorks, Inc., http://www.mathworks.com) to convert volume to area PSDs using the spherical scattering property kernel matrix provided by Sequoia Scientific. The size distributions were binned into 32 size bins ranging from 1.25 to $250 \, \mu\mathrm{m}$.

The MVFC was programmed to take images continuously with an image interval of 5 s. The MVFC took grayscale silhouette images of the suspended particles (Hill et al. 2011). Size analysis was performed with Image Processing and Analysis in Java (ImageJ, http://imagej.nih.gov/ij/). First, images were converted to binary images, using the triangle thresholding method (Zack et al. 1977). The outputs were analyzed in MATLAB to detect particles with circularity values larger than 0.6 (a value of 1.0 means a perfect circle). Elongated particles generally were diatom chains that were difficult to quantify precisely with the image analysis algorithms. By eliminating them from analysis, estimated areas were underestimates, but because visually elongated particles never made up a large fraction of the images, the trade-off between precision and accuracy was deemed acceptable. Nine pixels were chosen as the minimum number of pixels (3×3 pixels) to define a particle in an image, so the smallest particle resolved was approximately $36 \, \mu\mathrm{m}$ in diameter (Mikkelsen et al. 2006). The largest particle observed in the images was approximately $540 \, \mu\mathrm{m}$ in diameter. Particle areas and equivalent spherical diameters were subsequently computed and binned into 37 logarithmically increasing size bins that overlapped with bins 21–32 of the LISST.

Each MVFC area distribution was merged with its corresponding LISST particle area distribution. The LISST and MVFC particle size distributions overlapped across 12 bins with median diameters from 34 to $212 \, \mu\mathrm{m}$. The overlap size bins 21–23 were selected as the "merge bins." The proportion of area concentration from the LISST and from the MVFC in bin 21 was 75% and 25%, respectively. In size bins 22 and 23, the weight of the LISST area concentration decreased to 50% and 25%, and the weight of the MVFC area concentration increased to 50% and 75%, respectively. This weighted method produced a smooth interpolation from the LISST area concentration to the MVFC area concentration. The size bins 1–5 were omitted to mitigate the influence of "rising tails" in the LISST size spectrum (Mikkelsen et al.

2005). The merged particle area concentration distribution was formed with data from the LISST (bins 6–20), weighted data from the LISST and MVFC (bins 21–23), and data from the MVFC (bins 24–37). The TAC was calculated as the sum of all size bins of the merged area PSDs. The size measured size distribution extends from 2.85 to 540 μm, so it does not include the contribution of particles smaller than 2.85 μm or larger than 540 μm. It is assumed here that the calculated TAC is approximately equal to and proportional to the TAC of a size distribution that included particles smaller and larger than the instrumental limits. Schlieren had the largest effect on the accuracy of LISST estimates of large particle concentration (Styles 2006; Andrews et al. 2011). The merging algorithm, however, uses MVFC estimates of large particle concentrations, which minimizes the effect of schlieren on estimates of TAC.

SPM (g m^{-3}) was measured from water samples collected with Niskin bottles at 5- and 10-m depth and from water samples collected at the surface with a weighted open-mouthed 1-L sample bottle deployed by hand from the deck of the ship. Water samples were filtered through preweighed 8-μm Millipore SCWP (cellulose-acetate) filters on board the ship. These filters have effective pore sizes much smaller than 8 μm, and they are less prone to clogging than filters with smaller nominal pore sizes (Hill et al. 2013a). The filters were rinsed with distilled water to remove salts, and then dried and weighed in the laboratory.

The LISST-B measures c_p (m^{-1}) at 670 nm over a 5-cm pathlength. The instrument has an in-water acceptance angle of 0.027°. Because absorption of light by dissolved substances is generally small at 670 nm, the beam attenuation coefficient of the LISST was assumed to be equal to c_p (Hill et al. 2011; Neukermans et al. 2012). The WET Laboratories ac-9 (the acceptance angle is 0.93°), a combination of a spectral beam transmissometer and reflecting tube absorption meter, measures absorption and attenuation at nine wavelengths (λ: 412–715 nm), at 6 Hz (Twardowski et al. 1999; Slade and Boss 2015). An ac-9 requires a pump to pull the water into the sensing zone of the instrument. A flow-control switch (Sequoia Scientific FlowControl-Sub) allowed the ac-9 to collect either 0.2-μm filtered or raw water samples. For each profile, the instrument package was lowered into the water, and the ac-9 collected filtered water samples. When the instrument reached 1.5 m below the surface, the flow-control switch directed raw water into the intake of the ac-9. When the instrument reached a depth of 8 m, the switch was activated to direct the flow through the filter. The package continued to collect filtered water during the descent to the maximum depth of the profile and during the return

to the surface. Upon reaching 1.5 m on the second downcast in each profile, the flow-control switch changed to direct raw water into the instrument again. Another profile was collected in the same way, and after the second upcast the instrument package was recovered. Attenuation coefficients were corrected for temperature effect (Neukermans et al. 2012). The calibration-independent c_p(650 nm) was computed from the difference between total raw water beam attenuation (c_{pg}), which included water and dissolved plus particulate matter, and beam attenuation of water and the dissolved fraction smaller than 0.2 μm (c_g) (Boss et al. 2007). Even though the c_{pg} and c_g were collected from downcast and upcast profiles, respectively, it is assumed that the optical properties of the dissolved substances do not change between the down- and upcasts. In this study 40% of the c_g(715) exhibited values of 0.05 m^{-1} or higher, significantly larger than expected (near zero), which we attribute to bubbles. Those spectra were replaced with spectra reconstructed by regressing uncontaminated $c_g(\lambda)$ data with a CDOM fluorescence measured from a WET Laboratories WETStar CDOM fluorometer and salinity measured from a Sea-Bird 37 CTD. The CDOM and salinity are linearly correlated with $c_g(\lambda)$ in estuarine systems (Wang and Xu 2012), so the derived linear regressions were averaged to provide an estimated $c_g(\lambda)$.

The particulate attenuation spectra from an ac-9 typically follow a power-law distribution. To identify attenuation coefficients affected by spikes associated with bubbles and rare larger particles, each spectrum was fitted to a power law, and the coefficients of determination (R^2) were calculated. In this study, the 13% of spectra that had power-law fits with values of R^2 less than 0.95 were excluded. This method removed values of c_p(650) that were anomalously high or low relative to neighboring spectral values.

The WET Laboratories ECO bb2fl measures the volume-scattering function at a fixed angle in the backward direction (124°), at wavelengths of 532 and 650 nm. The volume-scattering function of particles was used to compute the particulate backscattering coefficient, b_{bp}(m^{-1}), following Boss et al. (2004) and Slade and Boss (2015). The b_{bp}(650) was used in this study. The median values of c_p(670), c_p(650), and b_{bp}(650) were derived in each 1-m depth bin from the surface to 10-m depth. As with optical data, a median binning procedure minimizes the contribution of spikes in the data associated with bubbles or rare large particles, because those spikes are not normally distributed in time or space (Whitmire et al. 2007; Boss et al. 2009b).

The buoyancy frequency, N (s^{-1}), was used to define the likelihood of schlieren (Mikkelsen et al. 2008;

Karageorgis et al. 2015). The N was computed from RBR CTD data as (Thomson and Emery 2014)

$$N = \left(-\frac{g}{\rho_0}\frac{\partial\rho}{\partial z}\right)^{0.5}, \tag{1}$$

where g (m s^{-2}) is the gravitational acceleration, ρ_0 (kg m^{-3}) is the average density during the downward profiling for each station, and $\partial\rho/\partial z$ is the vertical density gradient. To compare with optical proxies, TAC and N were bin averaged into 1-m depth bins from the surface to 10-m depth.

Model II regression has often been used to estimate the functional relationship between two field-observed variables in many oceanographic studies (Richter and Stavn 2014). Model II regression analysis was used between particle properties (PP) and optical properties (OP) to devise a model to predict PP from OP in this study. We used the MATLAB program *gmregress.m* for the model II regression (http://www.mathworks.com/matlabcentral/fileexchange/27918-gmregress). Goodness of fit and the statistical significance of the regression model are characterized with the correlation coefficient (r), the p value, and the normalized root-mean-square deviation (NRMSD), defined as

$$\text{NRMSD} = \frac{\left[\frac{1}{n}\sum_{i=1}^{n}(\hat{y}_i - y_i)^2\right]^{\frac{1}{2}}}{\max(y) - \min(y)}, \tag{2}$$

where y_i, $\hat{y}_i$, and n are the measured data, the regression estimate, and the number of data, respectively (Slade and Boss 2015).

3. Results

For particles that are large relative to the wavelength of light, the c_p and b_{bp} should be linearly proportional to the projected area concentration of particles in suspension (Beardsley et al. 1970). A linear relationship between c_p^{LISST} and TAC was obtained for the LISST only when observations with $N \leq 0.05\,\text{s}^{-1}$ were included (Fig. 1a). The linear relationship broke down for larger values of N. In contrast, the c_p^{ac9} from the pumped ac-9 and the b_{bp} from the bb2fl were linearly correlated with TAC over the entire range of buoyancy frequencies (Figs. 1b and 1c). Because the CRE is highly stratified, 35 profiles (80% of all profiles) exhibited stratification with $N > 0.05\,\text{s}^{-1}$, and valid c_p^{LISST} (observation $n = 143$) made up only 42% of all measurements. The larger sample size for the backscattering measurements ($n = 346$) compared to the ac-9 measurements ($n = 233$) was due to the sampling protocol of filtered versus unfiltered
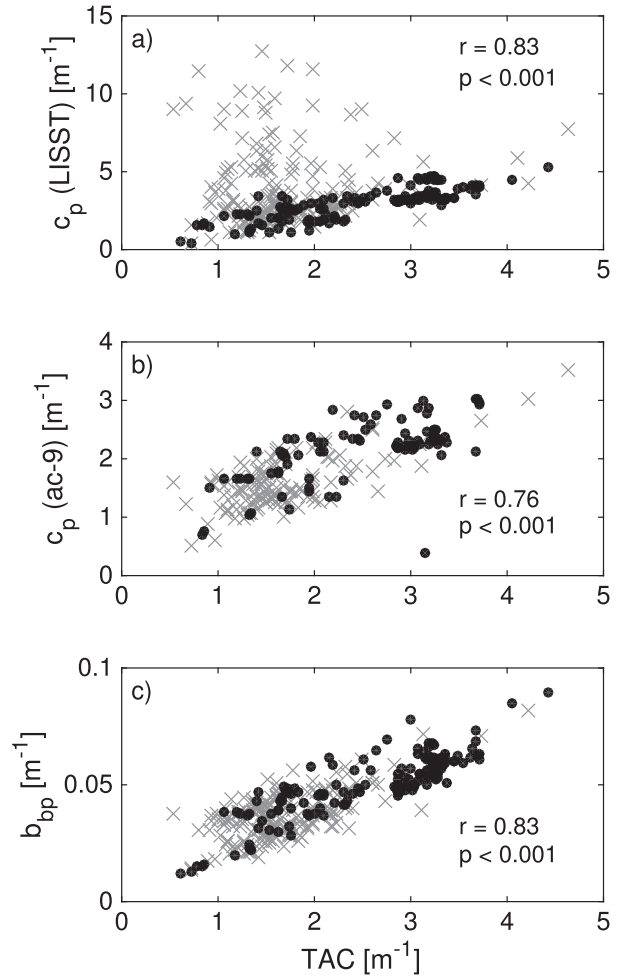
FIG. 1. Scatterplots of 1-m bin-averaged TAC (m^{-1}) with OP (m^{-1} for c_p and b_{bp}) derived from (a) a LISST, (b) an ac-9, and (c) a bb2fl. The c_p^{LISST} with $N \leq 0.05\,\text{s}^{-1}$ is well correlated with TAC, and c_p^{ac9} and b_{bp} are strongly correlated with TAC for the full range of N. Data collected when $N > 0.05\,\text{s}^{-1}$ (gray ×) and $N \leq 0.05\,\text{s}^{-1}$ (black dot). Term r is between TAC and c_p^{LISST} when $N \leq 0.05\,\text{s}^{-1}$, and the correlation coefficient between TAC and c_p^{ac9}, b_{bp} is over the entire range of N. The goodness of fit and the statistical significance of regression are expressed as r and p values, respectively.

samples for the ac-9. During downcasts, raw water was sampled only between 1.5- and 8-m water depths, so estimates of c_p^{ac9} were restricted to these depths. Optical backscattering coefficients were available for the entire depth of each downcast, which was always greater than 8 m.

The measured OP were correlated with SPM (Fig. 2). Note that only observations of c_p^{LISST} for which $N \leq 0.05\,\text{s}^{-1}$ are shown. Model II regression analysis between log(SPM) and log(OP) was used to devise a model to predict SPM from OP. All p values were less than 0.001, so the correlations are statistically highly significant between OP and SPM. The c_p^{ac9}-based SPM and the b_{bp}-based SPM models performed better, with
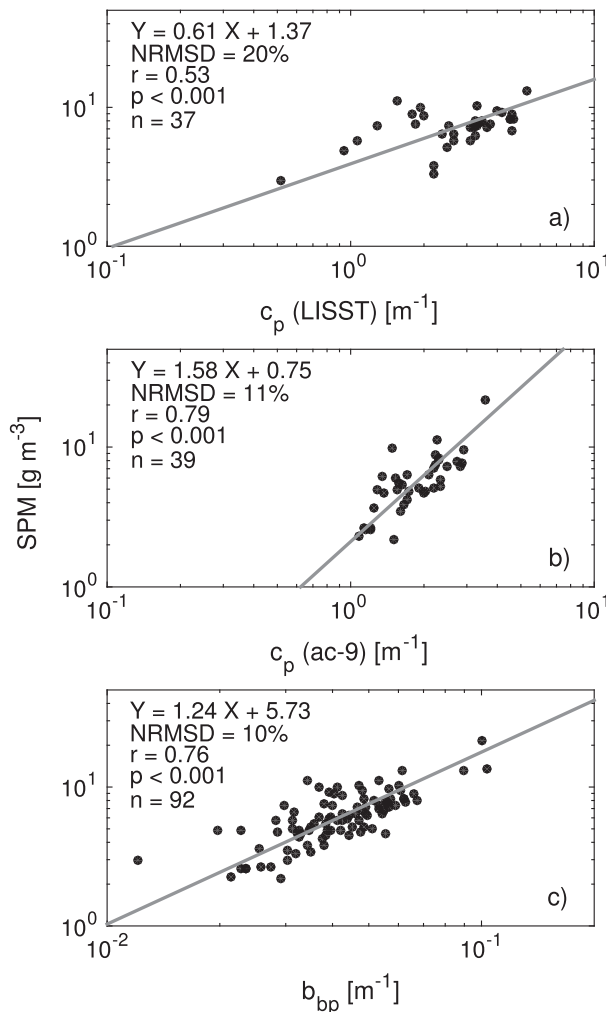
FIG. 2. Scatterplots of SPM ($g\,m^{-3}$) vs 1-m bin-averaged OP (m^{-1} for c_p and b_{bp}) derived from a LISST, an ac-9, and a bb2fl in the CRE transects in log–log space. Term c_p obtained from the LISST only when observations with $N \leq 0.05\,s^{-1}$ were included. The model II regression line is shown, with its equation and statistics. The X indicates the log(OP) and Y indicates the log(SPM).

FIG. 3. Example profiles of potential density ($kg\,m^{-3}$) and SPM ($g\,m^{-3}$) derived from OP, collected at a station near the mouth of the CRE, on 2 Jun 2013. Shown are density (black dotted line); SPM derived from a LISST (curve with open circles), an ac-9 (curve with squares), and a bb2fl (curve with triangles), using equations listed in Fig. 2; SPM from water samples (asterisks); and the depth range where $N > 0.05\,s^{-1}$ (shaded area). The LISST regression equation was from data for which $N \leq 0.05\,s^{-1}$, but for the profile here, the equation was applied to all c_p^{LISST} in order to calculate SPM. The effect of LISST overestimating SPM is typical of profiles that have high stratification.

correlation coefficients of 0.79 and 0.76 respectively, compared to a correlation coefficient of 0.53 for the c_p^{LISST}-based regression. Similarly, the NRMSD of c_p^{ac9} and b_{bp} were 11% and 10%, respectively, while the NRMSD of c_p^{LISST} was 20%.

The model II regression equations (listed in Fig. 2) were used to predict the SPM vertical profiles from LISST, ac-9, and bb2fl data at a station near the CRE mouth (Fig. 3). The profiles of SPM derived from the ac-9 and bb2fl were similar. Concentrations of approximately $5\,g\,m^{-3}$ occurred at 1-m depth. Concentrations rose at deeper depths, peaking at values near $10\,g\,m^{-3}$ at 5 m. Below 5 m, concentrations returned to values similar to those observed at the surface. This pattern was
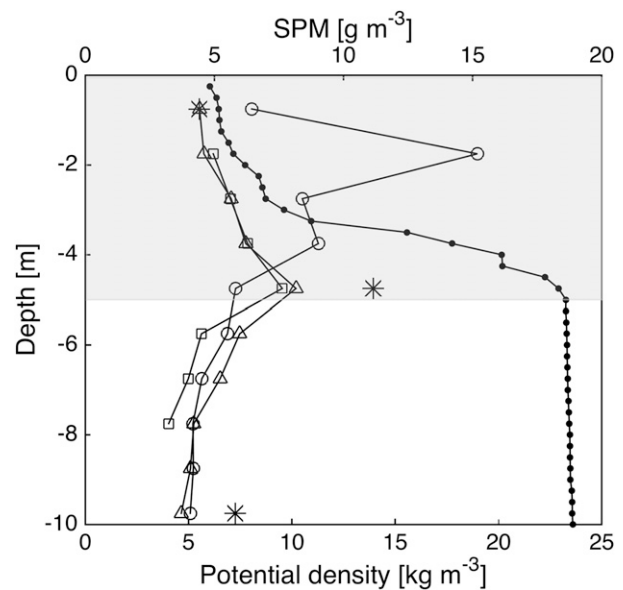
consistent with the SPM derived from water samples. The highest concentration was observed at 5 m, and the surface and 10-m samples had similar concentrations that were approximately 2 times smaller. The concentration profile generated from LISST data, without regard for potential error at depths with larger buoyancy frequencies, presented a much different profile of SPM, with a $15\,g\,m^{-3}$ peak located at the top of the pycnocline at 2 m, another smaller peak at 4 m, and no peak at 5 m.

4. Discussion and conclusions

High beam attenuations measured with open-path transmissometers in stratified waters may have been misinterpreted as particle-rich layers in past studies (e.g., Kistner and Pettigrew 2001; Jones et al. 2002; Lorenzoni et al. 2009). In this study c_p from a pumped transmissometer and b_{bp} from an optical backscatter sensor were not affected by stratification and provided accurate proxies for SPM. In the ac-9, density gradients were mixed in the intake tubes, which destroyed the conditions for schlieren to form. Although pumping water through the sensor's tube may have broken fragile

aggregates, c_p in the pumped sample was still proportional to SPM because the mass-normalized attenuation coefficients are weakly sensitive to size changes resulting from aggregation or disaggregation (Boss et al. 2009a; Hill et al. 2011; Slade et al. 2011). In addition, the ac-9 has a larger acceptance angle that weakens the influence of schlieren. The particulate backscattering coefficient is another useful proxy for SPM in stratified waters, because backscattered light is not affected by schlieren. Side-scattering instruments also should not be affected by schlieren, and previous work has shown that the side-scattering coefficient correlates with SPM (Boss et al. 2009c; Neukermans et al. 2012).

Particulate backscatter is the preferred proxy for SPM for stratified waters. The backscattering instrument was easy and convenient to operate. The optical backscatter sensor measured in situ optical properties, as opposed to optical properties of water that had been pumped into the sensing zone of the ac-9. In general, backscattering measurement uncertainties were lower than ac-9 measurement uncertainties, because the ac-9 measured c_{pg} and c_g with and without a prefilter. Changes in filter efficiency with time and colored dissolved material concentration at depth between profiles both increase the uncertainties (Boss et al. 2007). It is noted that the absorption and scattering by the dissolved substances does not contribute significantly to the attenuation at red bands, so a pumped single-band transmissometer with a red source would suffice for SPM estimation and would not require using the filtered/unfiltered method. However, the ac-9 filter efficiency should be considered for calculating spectral slopes of the particulate beam attenuation. In addition, the backscatter sensor is smaller than the ac-9 spectrophotometer and is light in weight. Together, these various advantages of the backscatter sensor made b_{bp} a better predictor of SPM than c_p^{ac9} in this study, which was consistent with previous studies (Boss et al. 2009c; Neukermans et al. 2012).

Schlieren affected the PSD of the area concentration (AC) and produced errors in LISST PSD. The scattering of light by schlieren onto the inner rings of the LISST results in erroneous estimates of high concentrations of large particles. Smaller sizes also were affected by the schlieren. PSDs of small particles produced by LISST were more peaked in stratified waters (Figs. 4c and 4d). The MVFC area PSDs obtained from two images with and without schlieren effects were not sensitive to schlieren (Figs. 4c and 4d). Four different calculated TACs highlight the responses of the instruments to schlieren (Table 1): the sum of LISST area PSD with particle size $< 36 \mu m$ (TAC_s^{LISST}), the sum of LISST area PSD with particle size $\geq 36 \mu m$ (TAC_l^{LISST}), the sum of

MVFC area PSD (TAC^{MVFC}), and the sum of the merged area PSD (TAC^{merged}). For the size distributions affected by schlieren, the LISST inversion of the scattered light indicated that there was more than 10 times as much area in particles larger than $36 \mu m$ than in particles smaller than $36 \mu m$. In contrast, the MVFC area of particles larger than $36 \mu m$ was of similar magnitude to the LISST estimate of area for particles less than $36 \mu m$. For the size distributions unaffected by schlieren, the areas estimated by LISST for small and large particles and by the MVFC for large particles all were of similar magnitude. Interestingly, despite the peaked shape of the LISST size distribution of small particles estimated in the presence of schlieren, the overall fraction of the total merged area represented by small particles was similar in the schlieren- and non-schlieren-affected data. As a result, the estimated TACs were not grossly inaccurate in stratified waters, despite relying on LISST data. A possible explanation is proposed for this observation. Schlieren and large particles scattered light primarily onto the inner rings of the LISST, leading to significant overestimation of the concentration of large particles when schlieren were present. Schlieren did not scatter light onto the outer rings, which the LISST inversion relies on to estimate the concentration of smaller particles. As a result, small particle concentrations were not grossly inaccurate. The size distribution was affected however because the LISST inversion assumes that large particles have associated secondary peaks on the outer rings (Davies et al. 2012). If schlieren did not produce similar secondary peaks, then the LISST inversion erroneously would assign some of the scattered light to the outer rings to large particles rather than to the small particles that actually caused the scattering.

Based on the data presented here, a buoyancy frequency of $0.05 \, s^{-1}$ is the appropriate threshold for schlieren effects in the CRE. Mikkelsen et al. (2008) and Karageorgis et al. (2015) suggested buoyancy frequencies above $0.025 \, s^{-1}$ and $0.01 \, s^{-1}$ were associated with increases in c_p due to schlieren effects. The suggested N threshold for the schlieren influence in the CRE is higher. The buoyancy frequencies were bin averaged, and the median c_p was chosen in a 1-m depth bin in this study, which may be the reason for the higher threshold value of N. This critical value of N depends on the size of the depth bin chosen for averaging and the LISST type. Different LISSTs have different acceptance angles. Because the CRE is an energetic estuary, profiling the instrument package may result in mixing of the stratified water in its wake. If the schlieren were destroyed at low buoyancy frequencies by the effect of the profiling package, then higher threshold values of N may result
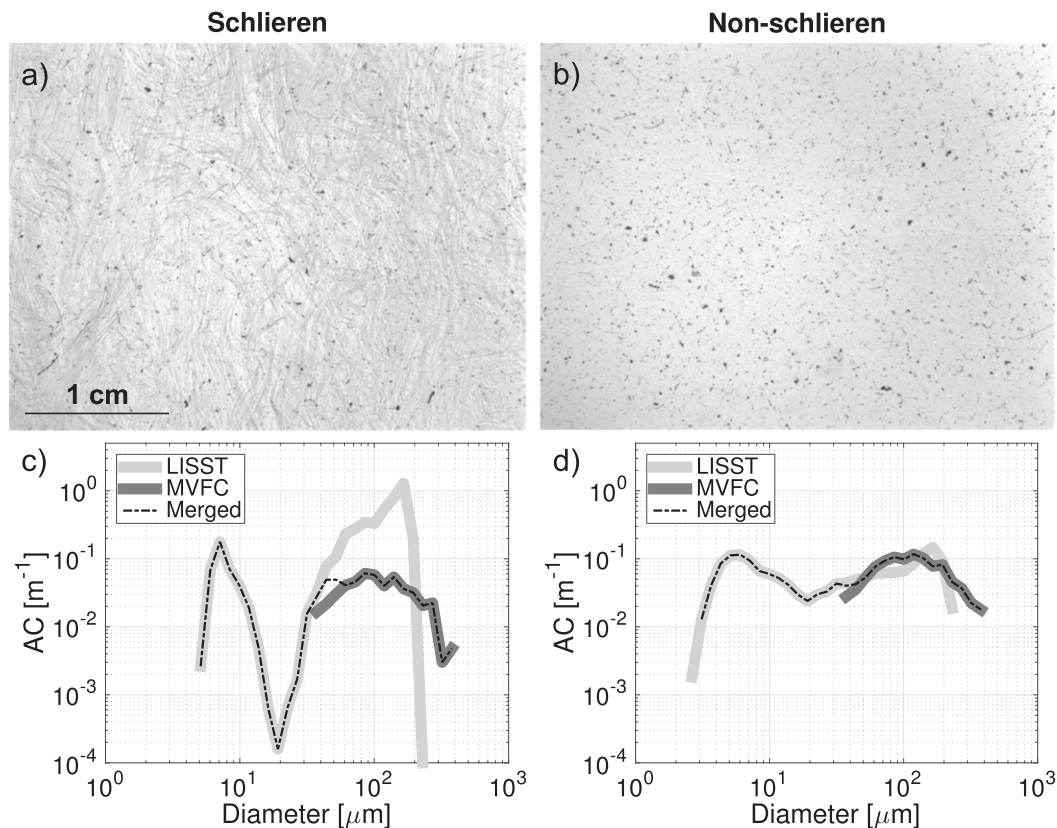
FIG. 4. MVFC images obtained (a) with widespread schlieren effects and b) without schlieren effects at two depths in a profile near the estuary mouth. (c),(d) Each MVFC area distribution was merged with its corresponding LISST particle area distribution. The PSD of AC (m^{-1}) estimated from the LISST (light gray curve), the MVFC (dark gray curve), and the two merged (dashed–dotted curves).

([Karageorgis et al. 2015](#)). Furthermore, observations in this study were at times from a stationary vessel in high currents and widespread schlieren effects still were observed, so towing a package would not necessarily mix water completely. Despite the fact that the threshold buoyancy frequency used in this study is higher, valid c_p values from the LISST were obtained for less than half of all measurements.

In this study, an appropriate threshold for the buoyancy frequency was provided for schlieren effects in LISST-100x-B. However, that threshold will vary depending on the acceptance angle of the optical instrument that is used. More research is necessary, either theoretical or laboratory-based work, to quantify the

definition of "small" acceptance angle that are prone to schlieren effects at buoyancy frequencies typically encountered in the ocean.

Stratification is a necessary condition for the formation of schlieren, but alone it is not sufficient. A source of energy for mixing is also required. In the CRE, mixing energy comes either from natural velocity shear or from the turbulence generated by flow past the instrument package. Both types of shear stress could be intermittent, because they all depend on variation in flow. Therefore, a large density gradient is no guarantee of schlieren presence. Schlieren effects would not occur systematically or necessarily in the most stratified part of the pycnocline. For example, in the cast depicted in

TABLE 1. Summary of TACs (m^{-1}) calculated from LISST PSDs, MVFC PSDs, and merged PSDs at two depths with and without shclieren effects as in [Figs. 4a and 4b](#), respectively. The TAC estimated from LISST PSD is separated into two groups by the particle size less (more) than 36 μm.

MVFC images	Depth (m)	TAC$_s^{\text{LISST}}$ ($<36\,\mu$m)	TAC$_l^{\text{LISST}}$ ($\geq36\,\mu$m)	TAC$^{\text{MVFC}}$ ($\geq36\,\mu$m)	TAC$^{\text{merged}}$ (full size)
Schlieren	2.69	0.4016	4.2098	0.4863	0.9455
Nonschlieren	7.72	0.8395	0.8594	0.9900	1.8484

Fig. 3, the highest peak of the SPM generated from LISST did not coincide with the strongest variation in the density gradient. The maximum schlieren effects occurred at the top of the pycnocline where stratification was not the most intense, while weaker effects occurred in the most stratified part. In addition, both reasonable and unreliable measurements of c_p^{LISST} were observed for $N > 0.05\,\text{s}^{-1}$ (gray $\times$ in Fig. 1a).

Particle dynamics in stratified waters affect the transfer of material from terrestrial to marine environments. Accurate characterization of these dynamics requires accurate proxies of SPM. Open-path transmissometers with small acceptance angles can suffer from significant loss of spatial and temporal coverage in data as a result of the effects of schlieren. Backscatter sensors represent a better tool because they are relatively simple to deploy and they are not affected by schlieren. We recommend the use of c_p in pumped sensors or b_{bp} as proxies for SPM in stratified waters.

REFERENCES

Andrews, S., D. Nover, J. Reuter, and S. Schladow, 2011: Limitations of laser diffraction for measuring fine particles in oligotrophic systems: Pitfalls and potential solutions. *Water Resour. Res.*, **47**, W05523, doi:10.1029/2010WR009837.

Beardsley, G. F., H. Pak, K. Carder, and B. Lundgren, 1970: Light scattering and suspended particles in the eastern equatorial Pacific Ocean. *J. Geophys. Res.*, **75**, 2837–2845, doi:10.1029/JC075i015p02837.

Boss, E., W. Pegau, M. Lee, M. Twardowski, E. Shybanov, G. Korotaev, and F. Baratange, 2004: Particulate backscattering ratio at LEO 15 and its use to study particle composition and distribution. *J. Geophys. Res.*, **109**, C01014, doi:10.1029/2002JC001514.

——, R. Collier, W. Pegau, G. Larson, and K. Fennel, 2007: Measurements of spectral optical properties and their relation to biogeochemical variables and processes in Crater Lake, Crater Lake National Park, OR. *Long-Term Limnological Research and Monitoring at Crater Lake, Oregon*, G. L. Larson, R. Collier, and M. W. Buktenica, Eds., Developments in Hydrobiology, Vol. 191, Springer, 149–159, doi:10.1007/978-1-4020-5824-0_9.

——, W. H. Slade, and P. Hill, 2009a: Effect of particulate aggregation in aquatic environments on the beam attenuation and its utility as a proxy for particulate mass. *Opt. Express*, **17**, 9408–9420, doi:10.1364/OE.17.009408.

——, ——, M. Behrenfeld, and G. Dall'Olmo, 2009b: Acceptance angle effects on the beam attenuation in the ocean. *Opt. Express*, **17**, 1535–1550, doi:10.1364/OE.17.001535.

——, and Coauthors, 2009c: Comparison of inherent optical properties as a surrogate for particulate matter concentration in coastal waters. *Limnol. Oceanogr. Methods*, **7**, 803–810, doi:10.4319/lom.2009.7.803.

——, L. Guidi, M. J. Richardson, L. Stemmann, W. Gardner, J. K. Bishop, R. F. Anderson, and R. M. Sherrell, 2015: Optical techniques for remote and in-situ characterization of particles pertinent to GEOTRACES. *Prog. Oceanogr.*, **133**, 43–54, doi:10.1016/j.pocean.2014.09.007.

Bottom, D. L., C. A. Simenstad, J. Burke, A. M. Baptista, D. A. Jay, K. K. Jones, E. Casillas, and M. H. Schiewe, 2005: Salmon at river's end: The role of the estuary in the decline and recovery of Columbia River salmon. NOAA Tech. Memo. NMFS-NWFSC-68, 246 pp.

Braithwaite, K., D. Bowers, W. N. Smith, G. Graham, Y. Agrawal, and O. Mikkelsen, 2010: Observations of particle density and scattering in the Tamar Estuary. *Mar. Geol.*, **277**, 1–10, doi:10.1016/j.margeo.2010.06.008.

Burchard, H., and H. Baumert, 1998: The formation of estuarine turbidity maxima due to density effects in the salt wedge. A hydrodynamic process study. *J. Phys. Oceanogr.*, **28**, 309–321, doi:10.1175/1520-0485(1998)028<0309:TFOETM>2.0.CO;2.

Davies, E. J., W. A. M. Nimmo-Smith, Y. C. Agrawal, and A. J. Souza, 2012: LISST-100 response to large particles. *Mar. Geol.*, **307–310**, 117–122, doi:10.1016/j.margeo.2012.03.006.

Elias, E. P., G. Gelfenbaum, and A. J. Van der Westhuysen, 2012: Validation of a coupled wave-flow model in a high-energy setting: The mouth of the Columbia River. *J. Geophys. Res.*, **117**, C09011, doi:10.1029/2012JC008105.

Fugate, D. C., and C. T. Friedrichs, 2002: Determining concentration and fall velocity of estuarine particle populations using ADV, OBS and LISST. *Cont. Shelf Res.*, **22**, 1867–1886, doi:10.1016/S0278-4343(02)00043-2.

Hill, P. S., C. Sherwood, R. Sternberg, and A. Nowell, 1994: *In situ* measurements of particle settling velocity on the northern California continental shelf. *Cont. Shelf Res.*, **14**, 1123–1137, doi:10.1016/0278-4343(94)90031-0.

——, E. Boss, J. Newgard, B. Law, and T. Milligan, 2011: Observations of the sensitivity of beam attenuation to particle size in a coastal bottom boundary layer. *J. Geophys. Res.*, **116**, C02023, doi:10.1029/2010JC006539.

——, J. Newgard, B. Law, and T. Milligan, 2013a: Flocculation on a muddy intertidal flat in Willapa Bay, Washington, Part II: Observations of suspended particle size in a secondary channel and adjacent flat. *Cont. Shelf Res.*, **60**, S145–S156, doi:10.1016/j.csr.2012.06.006.

——, D. G. Bowers, and K. M. Braithwaite, 2013b: The effect of suspended particle composition on particle area-to-mass ratios in coastal waters. *Methods Oceanogr.*, **7**, 95–109, doi:10.1016/j.mio.2014.02.003.

Jones, B. H., M. A. Noble, and T. D. Dickey, 2002: Hydrographic and particle distributions over the Palos Verdes Continental Shelf: Spatial, seasonal and daily variability. *Cont. Shelf Res.*, **22**, 945–965, doi:10.1016/S0278-4343(01)00114-5.

Kappenberg, J., G. Schymura, and H.-U. Fanger, 1995: Sediment dynamics and estuarine circulation in the turbidity maximum of the Elbe River. *Neth. J. Aquat. Ecol.*, **29**, 229–237, doi:10.1007/BF02084220.

Karageorgis, A., D. Georgopoulos, W. Gardner, O. Mikkelsen, and D. Velaoras, 2015: How schlieren affects beam transmissometers and LISST-Deep: An example from the stratified Danube River delta, NW Black Sea. *Mediterr. Mar. Sci.*, **16**, 366–372, doi:10.12681/mms.1116.

Kistner, D. A., and N. R. Pettigrew, 2001: A variable turbidity maximum in the Kennebec estuary, Maine. *Estuaries*, **24**, 680–687, doi:10.2307/1352876.

Lorenzoni, L., and Coauthors, 2009: The importance of subsurface nepheloid layers in transport and delivery of sediments to the eastern Cariaco Basin, Venezuela. *Deep-Sea Res. I*, **56**, 2249–2262, doi:10.1016/j.dsr.2009.08.001.

Mikkelsen, O. A., P. S. Hill, T. G. Milligan, and R. J. Chant, 2005: In situ particle size distributions and volume concentrations from a LISST-100 laser particle sizer and a digital floc camera. *Cont. Shelf Res.*, **25**, 1959–1978, doi:10.1016/j.csr.2005.07.001.

——, ——, and ——, 2006: Single-grain, microfloc and macrofloc volume variations observed with a LISST-100 and a digital floc camera. *J. Sea Res.*, **55**, 87–102, doi:10.1016/j.seares.2005.09.003.

——, T. G. Milligan, P. S. Hill, R. J. Chant, C. F. Jago, S. E. Jones, V. Krivtsov, and G. Mitchelson-Jacob, 2008: The influence of schlieren on in situ optical measurements used for particle characterization. *Limnol. Oceanogr. Methods*, **6**, 133–143, doi:10.4319/lom.2008.6.133.

Neukermans, G., H. Loisel, X. Mériaux, R. Astoreca, and D. McKee, 2012: In situ variability of mass-specific beam attenuation and backscattering of marine particles with respect to particle size, density, and composition. *Limnol. Oceanogr.*, **57**, 124–144, doi:10.4319/lo.2012.57.1.0124.

North, E., S. Chao, L. Sanford, and R. Hood, 2004: The influence of wind and river pulses on an estuarine turbidity maximum: Numerical studies and field observations in Chesapeake Bay. *Estuaries*, **27**, 132–146, doi:10.1007/BF02803567.

Pak, H., and J. R. V. Zaneveld, 1977: Bottom nepheloid layers and bottom mixed layers observed on the continental shelf off Oregon. *J. Geophys. Res.*, **82**, 3921–3931, doi:10.1029/JC082i027p03921.

Puig, P., A. Palanques, J. Guillén, and M. El Khatab, 2004: Role of internal waves in the generation of nepheloid layers on the northwestern Alboran slope: Implications for continental margin shaping. *J. Geophys. Res.*, **109**, C09011, doi:10.1029/2004JC002394.

Richter, S. J., and R. H. Stavn, 2014: Determining functional relations in multivariate oceanographic systems: Model II multiple linear regression. *J. Atmos. Oceanic Technol.*, **31**, 1663–1672, doi:10.1175/JTECH-D-13-00210.1.

Schoellhamer, D. H., and S. A. Wright, 2003: Continuous measurement of suspended-sediment discharge in rivers by use of optical backscatterance sensors. *Erosion and Sediment Transport Measurement in Rivers: Technological and Methodological Advances*, J. Bogen, T. Fergus, and D. Walling, Eds., IAHS Publ. 283, 28–36.

Slade, W. H., and E. Boss, 2015: Spectral attenuation and backscattering as indicators of average particle size. *Appl. Opt.*, **54**, 7264–7277, doi:10.1364/AO.54.007264.

——, ——, and C. Russo, 2011: Effects of particle aggregation and disaggregation on their inherent optical properties. *Opt. Express*, **19**, 7945–7959, doi:10.1364/OE.19.007945.

Styles, R., 2006: Laboratory evaluation of the LISST in a stratified fluid. *Mar. Geol.*, **227**, 151–162, doi:10.1016/j.margeo.2005.11.011.

Thomson, R. E., and W. J. Emery, Eds, 2014: *Data Analysis Methods in Physical Oceanography*. 3rd ed. Elsevier, 637 pp.

Traykovski, P., R. Geyer, and C. Sommerfield, 2004: Rapid sediment deposition and fine-scale strata formation in the Hudson estuary. *J. Geophys. Res.*, **109**, F02004, doi:10.1029/2003JF000096.

Twardowski, M. S., J. M. Sullivan, P. L. Donaghay, and J. R. V. Zaneveld, 1999: Microscale quantification of the absorption by dissolved and particulate material in coastal waters with an ac-9. *J. Atmos. Oceanic Technol.*, **16**, 691–707, doi:10.1175/1520-0426(1999)016<0691:MQOTAB>2.0.CO;2.

Wang, F., and Y. J. Xu, 2012: Remote sensing to predict estuarine water salinity. *Environmental Remote Sensing and Systems Analysis*, CRC Press, 85–108.

Whitmire, A. L., E. Boss, T. J. Cowles, and W. S. Pegau, 2007: Spectral variability of the particulate backscattering ratio. *Opt. Express*, **15**, 7019–7031, doi:10.1364/OE.15.007019.

Xi, H., P. Larouche, S. Tang, and C. Michel, 2014: Characterization and variability of particle size distributions in Hudson Bay, Canada. *J. Geophys. Res. Oceans*, **119**, 3392–3406, doi:10.1002/2013JC009542.

Zack, G., W. Rogers, and S. Latt, 1977: Automatic measurement of sister chromatid exchange frequency. *J. Histochem. Cytochem.*, **25**, 741–753, doi:10.1177/25.7.70454.